Fish-Eye Imaging With A LOFAR Station

Stefan J. Wijnholds
ASTRON, Oude Hoogeveensedijk 4, NL-7991 PD, Dwingeloo, The Netherlands
Tel: +31 521 595 261, e-mail: wijnholds@astron.nl

I. Introduction

The radio astronomical community is currently making detailed plans for the construction of the square kilometer array (SKA) [3]. Survey speed, i.e. the time in which a certain fraction of the sky can be mapped out for a given sensitivity, is a key figure of merit for the SKA. As a result, all instrument concepts currently under investigation have a large field of view (FOV). A large FOV implies that projection effects due to the non-planarity of the celestial sphere within the FOV can no longer be ignored. This complicates the imaging routines, which have to disentangle the true image of the sky from instrumental effects, such as the antenna and array sensitivity patterns, and environmental effects, such as ionospheric and tropospheric distortions, a process called deconvolution. Another complicating factor is that some science cases, such as the study of galactic magnetic fields and the early universe, require imaging of very complicated source structures, while standard imaging routines are tailored to point sources. An overview of imaging methods can be found in [2].

These methods were originally developed for arrays with a small FOV to deconvolve fields containing mainly point sources. For such fields, these methods were computationally efficient since they could rely on the fast Fourier transform. They can still be used to map out large FOVs if the image is subdivided into smaller subimages (facets) over which the algorithm can iterate. More complex source structures can be handled by making images at different resolutions as done in methods such as multi-resolution CLEAN. Iterations over distinct resolution scales and facets make these methods more computationally intensive while convergence has not been demonstrated for all cases. This is problematic for instruments with all-sky, i.e. 2π steradian, imaging capabilities, such as an aperture array station. This challenge can be handled by following a model based imaging approach in which imaging is treated as a parameter estimation problem. In this paper, image parameters are estimated using least squares optimization, but other optimizations could be considered as well [5]. These parametric methods generally have a numerical complexity of $O\left(Q^3\right)$ where Q is the number of image points, while existing algorithms have iterations with a complexity of $O\left(Q^2\right)$. However, the latter may not be faster if the number of iterations becomes very large. Furthermore, convergence of these iterative methods is not always guaranteed. With modern computing hardware, the optimal choice of method should thus be drive by the challenges of the imaging problem and not on the limitations imposed by the computing hardware.

II. Model based calibration and imaging

A radio telescope array measures the spatial coherency of the incoming electromagnetic field by correlating the signals received by its P antennas. These P^2 correlations, referred to as visibilities, can be stacked in a $P^2 \times 1$ vector $\mathbf{v}$. The coherency function is the result of a superposition of Q source signals. An image of the sky can be regarded as a collection of point sources, each source representing a pixel in the image. The source powers σ_q can be stacked in a $Q \times 1$ vector $\boldsymbol{\sigma}_n$. The relation between the visibilities and the source powers, i.e. the measurement equation or data model, is given by [10]

$$\mathbf{v} = \mathbf{M}\boldsymbol{\sigma} + \mathbf{n}, \tag{1}$$

where $\mathbf{M}$ is the $P^2 \times Q$ instrument matrix, which describes all instrumental and environmental perturbations of the signal, and $\mathbf{n}$ is the $P^2 \times 1$ noise vector, which will be modeled as $\mathbf{n} = \mathbf{M}_n\boldsymbol{\sigma}_n$ with noise model $\mathbf{M}_n$ and parameterization $\boldsymbol{\sigma}_n$.

Based on (1), the imaging problem can be formulated as

$$\{\widehat{\boldsymbol{\sigma}}, \widehat{\boldsymbol{\sigma}}_n\} = \underset{\boldsymbol{\sigma},\boldsymbol{\sigma}_n}{\operatorname{argmin}} \left\| \mathbf{W}\left(\widehat{\mathbf{v}} - \mathbf{M}\boldsymbol{\sigma} - \mathbf{M}_n\boldsymbol{\sigma}_n\right)\right\|_F^2, \tag{2}$$

where $\mathbf{W}$ is a weighting matrix. The optimal statistical performance is achieved if $\mathbf{W}$ is chosen based on the data itself following a covariance matching approach [6]. This least squares image optimization is

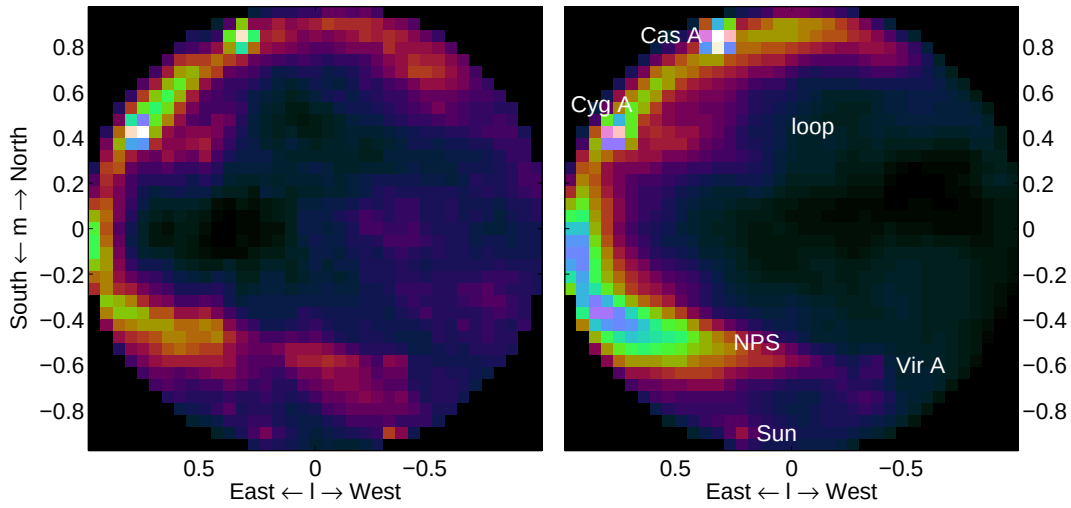

Fig. 1. These total intensity maps were made by combining data from 27 156 kHz frequency channels evenly distributed between 45.3 and 67.3 MHz and 10 seconds of integration per channel. The left panel shows the result after applying a direct Fourier transform to the raw visibility data followed by summation over frequency while the right panel shows the least squares imaging result obtained after calibration of the individual frequency channels.

also known as optimal map making [7], but other optimizations are also being considered [5]. The latter are very interesting for fields which are mainly empty and contain only point sources, i.e. for sparse data, since the least squares cost function is known to have poor performance for sparse data [1]. The advantage of a formulation in terms of linear algebra is that a full error and noise propagation analysis can be made [10].

We can solve (2) for $\boldsymbol{\sigma}_n$ and formulate the solution in terms of $\boldsymbol{\sigma}$:

$$\widehat{\boldsymbol{\sigma}}_n = (\mathbf{W}\mathbf{M}_n)^\dagger \mathbf{W} \left(\widehat{\mathbf{v}} - \mathbf{M}\boldsymbol{\sigma}\right) = \widetilde{\mathbf{M}}_n \left(\widehat{\mathbf{v}} - \mathbf{M}\boldsymbol{\sigma}\right), \tag{3}$$

where † denotes the pseudo-inverse. Substitution in (2) gives

$$\widehat{\boldsymbol{\sigma}} = \underset{\boldsymbol{\sigma}}{\operatorname{argmin}} \left\| \left(\mathbf{W} - \mathbf{W}\mathbf{M}_n\widetilde{\mathbf{M}}_n\right) \left(\widehat{\mathbf{v}} - \mathbf{M}\boldsymbol{\sigma}\right) \right\|_F^2 = \underset{\boldsymbol{\sigma}}{\operatorname{argmin}} \left\| \widetilde{\mathbf{W}}\widehat{\mathbf{v}} - \widetilde{\mathbf{W}}\mathbf{M}\boldsymbol{\sigma} \right\|_F^2, \tag{4}$$

which leads to the solution

$$\widehat{\boldsymbol{\sigma}} = \left(\widetilde{\mathbf{W}}\mathbf{M}\right)^\dagger \widetilde{\mathbf{W}}\widehat{\mathbf{v}} = \mathbf{M}_d^{-1}\boldsymbol{\sigma}_d. \tag{5}$$

Here we have introduced the $Q \times Q$ deconvolution matrix $\mathbf{M}_d = \mathbf{M}^H\widetilde{\mathbf{W}}^H\widetilde{\mathbf{W}}\mathbf{M}$ and the $Q \times 1$ dirty image vector $\mathbf{M}^H\widetilde{\mathbf{W}}^H\widetilde{\mathbf{W}}\widehat{\mathbf{v}}$. The dirty image is the true image perturbed by the instrumental and environmental effects described by the data model. The deconvolution matrix disentangles these effects and the true image leading to a reconstruction of the true image.

It is very important to note that the deconvolution matrix has size $Q \times Q$ and that the dirty image has size $Q \times 1$ regardless of the amount of data collected in $\widehat{\mathbf{v}}$. This even holds if many snapshot observations, i.e. observations covering a time and frequency span over which the instrument model can be assumed constant, are combined. This property makes this an attractive observing technique for very wide field imaging with relatively small arrays with complex source distributions, such as observation of magnetic fields in the Milky Way, the early universe or all sky transient monitoring. These are typical science cases considered for the inner parts of the low frequency array (LOFAR) [8] and SKA.

III. Results

Since the strong points of the proposed imaging technique are deconvolution of complex source structure and handling of an arbitrarily large field-of-view, it should be well suited for full sky imaging with a LOFAR station. On 8 November 2008 between 10:21:59 and 10:26:45 UTC data was captured

from 48 low band antennas on a LOFAR prototype station near Exloo (The Netherlands). Each antenna consists of two inverted V-shaped dipoles referred to as x- and y-dipole. A correlator was used to correlate 27 156 kHz wide RFI free frequency bands evenly distributed between 45.3 and 67.3 MHz. The integration time per band was set to 10 seconds. The arrays of x- and y-dipoles were calibrated independently using the weighted alternating least squares approach described in [11] using Cas A and Cyg A, the two brightest sources on the northern hemisphere at these frequencies, as calibrators. The least squares imaging technique was applied to the calibrated xx- and yy-visibilities separately. The final result is shown in Fig. 1. For comparison, the raw visibilities for each subband were transformed into an image by a direct Fourier transform (DFT, see e.g. [9]) before adding the images from the individual channels.

In the least squares image a number of well known sources have been indicated. The most subtle feature visible is the galactic loop emerging from Cygnus. This bit of extended emission can be identified as loop 3 in the Haslam survey [4]. This shows the improvement of the least squares image over the DFT image. In the DFT image, there is some extended emission emerging from Cygnus A, but there is also a large region of extended emission near the western horizon that can not be associated with known sources. In the least squares image, this emission disappears while the emission near Cygnus A remains. We can therefore conclude that the extended emission near the western horizon in the DFT image is actually caused by the instrumental response to the galactic plane and north polar spur. This demonstrates that least squares imaging adequately removes the instrumental responses thus showing only the real emission in the final image. This simple observation already includes an interesting deconvolution challenge since the image contains both strong point sources as well as extended emission. This would require at least a multi-resolution CLEAN taking into account the averaging of the array point spread function over the 27 distinct frequencies involved. The proposed least squares imaging technique performs this deconvolution task implicitly.

IV. Conclusions

The least squares imaging technique is a very promising technique for very wide field imaging of complex source structures with relatively small arrays. This was demonstrated for the extreme case of instantaneous full sky imaging with a LOFAR station. Its implicit deconvolution makes this technique very attractive for science cases with complex source structures such as study of the galactic magnetic fields and the very early universe and should thus be considered for observations with the inner parts of the SKA and LOFAR arrays.

References

[1] Emmanuel J. Candès and Michael B. Wakin. An Introduction to Compressive Sampling. *IEEE Signal Processing Magazine*, 25(2):21–30, March 2008.

[2] Tim J. Cornwell, Kumar Golap, and Sanjay Bhatnagar. The Noncoplanar Baselines Effect in Radio Interferometry: The W-Projection Algorith. *IEEE Journal of Selected Topics in Signal Processing*, 2(5):647–657, October 2008.

[3] P.J. Hall. The Square Kilometer Array: an International Engineering Perspective. *Experimental Astronomy*, 17(1-3):5–16, 2004.

[4] C.G.T. Haslam, C.J. Salter, H. Stoffel, and W.E. Wilson. A 408 MHz all-sky continuum survey II - The atlas of contour maps. *Astronomy and Astrophysics Supplement Series*, January 1982.

[5] R. Levanda and A. Leshem. Image Formation in Radio Astronomy. *IEEE Signal Processing Magazine*, 27(1), January 2010. in preparation.

[6] B. Ottersten, P. Stoica, and R. Roy. Covariance Matching Estimation Techniques for Array Signal Processing Applications. *Digital Signal Processing, A Review Journal*, 8:185–210, July 1998.

[7] Max Tegmark. How to Make Maps From Cosmic Microwave Background Data Without Losing Information. *Astrophysical Journal Letters*, 480:L87–L90, May 1997.

[8] M. de Vos, A.W. Gunst, and R. Nijboer. The LOFAR Telescope: System Architecture and Signal Processing. *IEEE Proceedings*, 2009. accepted for publication.

[9] Stefan J. Wijnholds, Jaap D. Bregman, and Albert-Jan Boonstra. Sky Noise Limited Snapshot Imaging in the Presence of RFI With LOFAR's Initial Test Station. *Experimental Astronomy*, 17(1-3):35–42, 2004.

[10] Stefan J. Wijnholds and Alle-Jan van der Veen. Fundamental Imaging Limits of Radio Telescope Arrays. *IEEE Journal of Selected Topics in Signal Processing*, 2(5):613–623, October 2008.

[11] Stefan J. Wijnholds and Alle-Jan van der Veen. Multisource Self-calibration for Sensor Arrays. *IEEE Transactions on Signal Processing*, 2009. in press.